www.sciencemag.org/content/351/6274/720/suppl/DC1

Supplementary Materials for

Dynamics of epigenetic regulation at the single-cell level

Lacramioara Bintu, John Yong, Yaron E. Antebi, Kayla McCue, Yasuhiro Kazuki, Narumi Uno, Mitsuo Oshimura, Michael B. Elowitz*

*Corresponding author. E-mail: melowitz@caltech.edu

Published 12 February 2016, *Science* **351**, 720 (2016)
DOI: 10.1126/science.aab2956

This PDF file includes:

Other Supplementary Material for this manuscript includes the following:
(available at www.sciencemag.org/content/351/6274/720/suppl/DC1)

Materials and Methods

Plasmid construction

The PhiC31-Neo-ins-5xTetO-pEF-H2B-Citrine-ins reporter construct (Fig. 1B) was assembled using a backbone containing the PhiC31 attB site, a neomycin resistance gene, and a multiple cloning site flanked by two 1.2kb chicken HS4 insulators (16) on each side (phiC31-Neomycin-2xcHS4ins-MCS-2xcHS4ins). Three elements of the reporter were PCR amplified from the following sources: five Tet binding sites from the TRE-tight plasmid (Clontech), pEF from pEF/FRT/V5-Dest (Life Technologies), and H2B-citrine from pEV2-12xCSL-H2B-Citrine (36). These components were first sequentially cloned into the pExchange1 backbone using standard molecular biology techniques. The entire TRE-pEF-H2B-citrine was then PCR-amplified and combined by Gibson assembly with the phiC31-Neomycin-2xcHS4ins-MCS-2xcHS4ins backbone cut by AvrII. This construct was designed such that after integration, the neomycin gene would be expressed from a PGK promoter situated upstream of the phiC31 site in the HAC (16). The PhiC31 integrase was a gift from the Oshimura Lab (16).

The plasmids containing the rTetR-CR fusions were built using Gibson assembly of the pExchange1 backbone containing the pEF promoter (cut with BamHI and KpnI), H2B-mCherry (PCR-amplified from a derivative of pEV-12xCSL-H2B-mCherry (36)), rTetR (PCR-amplified from rtTA3 system, Clontech), and a PCR product for each CR. The source plasmids encoding the CRs were as follows: pCMV-HA-EED (Addgene 24231), HDAC4 Flag (Addgene 13821), DNMT3B cDNA (isoform 5, OpenBiosystems MMM1013-99827219), and PSV40-E-KRAB-pA (pWW43 (37), a gift from Martin Fussenegger).

Cell line construction

The reporter line was created by integrating the H2B-citrine reporter site-specifically in an artificial chromosome (MI-HAC) in CHO-K1 cells (16). This system has several key advantages that make it ideal for single-cell analysis of gene expression dynamics during CR recruitment and release. Since CHO-K1 cells form a monolayer with well-separated nuclei, they are amenable to long-term time-lapse imaging for up to ~5 days, allowing us to characterize silencing and reactivation events in single cells. In addition, they can be passaged for more than 30 days, allowing long-term measurements of epigenetic memory. The MI-HAC lacks endogenous genes, thus minimizing unknown interactions between our reporter and other genes. Moreover, the MI-HAC can be transferred to different cell lines by microcell-mediated chromosome transfer (MMCT) (16), allowing one to quantify the effect of cell type on the dynamics of silencing and reactivation, while maintaining a constant genetic context.

Integration of the reporter was performed by co-transfecting 600 ng PhiC31-Neo-ins-5xTetO-pEF-H2B-Citrine-ins reporter plasmid and 200 ng PhiC31 integrase plasmid, using Lipofectamine 2000 (Invitrogen). The transfection was performed in 24-well plates. Cells were transferred to 6-well plates 24 hours later and selected with 400 ng/ul geneticin for 12 days, starting 40 hours after the transfection. Single clones were obtained by limiting dilution. The integration of the reporter in the HAC was verified by genomic PCR, and a single clone was chosen for further analysis.

Each of the CR plasmids (pEF-H2B-mCherry-T2A-rTet-CR) was randomly integrated into this reporter line by transfection with Lipofectamine 2000 (Invitrogen). These cells were selected using 300 µg/ml zeocin starting 24 hours after transfection for a total of 12 days. Finally, single clones were selected for each CR by limiting dilution.

Other Chromatin Regulators

In addition to the CRs presented in the main text (EED, KRAB, DNMT3B and HDAC4), we have also tested: EZH2, REST, HDAC3 and RNF2 (RING1B) (Fig. S12). For both EZH2 (part of PRC2) and REST, we observe all-or-none silencing of most cells after 5 days of recruitment. We did not observe any silencing upon HDAC3 recruitment, and very little silencing with RNF2.

Culture conditions

Cells were cultured at 37ºC, in a humidified atmosphere with 5% CO2. For all experiments, except movies, the growth media consisted of Alpha MEM Earle's Salts (9144, Irvine Scientific) with 10% Tet Approved FBS (Clontech Laboratories) and 1X Penicillin/Streptomycin/L-glutamine (Life Technologies) added. Media containing the appropriate antibiotics (300 µg/ml neomycin and 300 µg/ml zeocin) were changed every 2-3 days during maintenance. During movies, cells were grown in low-fluorescence imaging media (36), which consisted of Alpha-MEM without phenol red, riboflavin, folic acid, and vitamin B12 (Life Technologies, custom made), supplemented with 10% FBS and 1X Pen/Strep/L-glutamine. During all recruitment and de-recruitment experiments, media without neomycin or zeocin were used and changed every 24 hours in all wells. Cells were harvested by rinsing with Dulbecco's Phosphate-Buffered Saline (DPBS, Life Technologies), and incubating at room temperature with 0.25% Trypsin (Life Technologies). For long-term storage, cells were frozen in growth media with 10% DMSO, placed at -80ºC (for up to a month), and then transferred to liquid nitrogen.

Acquisition of time-lapse movies

Reporter cells expressing each of the four CRs were plated approximately 12 hours before imaging, at low density (1,500 cells/cm^2) on glass-bottom plates (MatTek) coated with 5 µg/ml hamster fibronectin (Oxford Biomedical Research). Imaging was done using an inverted Olympus IX81 fluorescence microscope with Zero Drift Control (ZDC), a 20X dry objective, and an iKon-M CCD camera (Andor, Belfast, NIR). Fluorophores were excited using an X-Cite XLED1 light source (Lumen Dynamics). Images were automatically acquired every 20 minutes, using Metamorph software (Molecular Devices). The microscope was enclosed in a chamber kept at 37ºC and 5% CO_2, and the imaging growth media (see Culture conditions) was changed daily. Silencing movies began with reporter cells actively expressing the reporter gene. Dox (1 µg/ml) was added to the cells at ~20 hours, after which imaging continued for at least 3 more days and until cell tracking became difficult due to high cell density. Cells were then re-plated at low density, in the presence of dox, for the subsequent acquisition of reactivation movies. Imaging began with these cells ~12 hours after re-plating, and dox was washed-out at ~20 hours into the movies (5 days since the beginning of dox addition).

Analysis of time-lapse data and silencing event detection

Cells were segmented and tracked using the mCherry fluorescence signal with custom Matlab code (available upon request), as follows: (1) Initially, images were processed to correct for inhomogeneous fluorescent illumination by fitting a paraboloid to background (non-cell) pixel intensities, and then normalizing the image by this paraboloid. (2) We then used an integrated segmentation and tracking procedure which combined (a) a pixel-based intensity threshold for segmentation, (b) a tracking algorithm based on global minimization of a cost function that incorporates cell positions and fluorescence intensities, and (c) heuristics that use discontinuities in tracking to correct segmentation. (3) Finally, all individual cell lineages were checked and corrected manually.

Using the contours obtained from this algorithm, total Citrine fluorescence levels were extracted for each of the cell lineages. Since the H2B-Citrine protein is stable, total fluorescence levels increased at a steady rate when the reporter was expressed at a constant level (Fig. 1C, '-dox'), but remained constant (flat) when the reporter gene was silenced. At each cell division, the total fluorescence signal was approximately halved as fluorescent protein molecules partitioned between daughter cells (*38*). We computationally restored the fluorescence lost during these division events by computing the lost fluorescence and adding this constant value to all subsequent time points after a division event. This procedure, repeated for all division events, generated the cumulative total fluorescence traces (Fig. 1C, solid line), from which reporter production rates were assessed (slope of solid line in Fig. 1C).

To detect silencing events, a threshold on reporter production rate was set for each individual lineage at 50% of its median before dox addition (Fig. S3A). To avoid mis-identification of silencing events due to fluctuations in gene expression levels, a cell was marked silent when its reporter production rate dropped and remained below this threshold for at least 12 hours.

Reactivation events were identified when the reporter production rate of a silent cell increased beyond a global threshold, and remained above this threshold for at least 12 hours (Fig. S6). This global threshold was set at 50% of the median reporter production rate of all cells before the initial dox addition. The rationale for using a global threshold instead of a lineage-specific threshold for reactivation movies is that cells start these movies at zero production rate and in many cases do not reactivate during the movie. As a result, for many lineages, there is no natural lineage-specific threshold.

ChIP-qPCR and MeDIP-qPCR

Each cell line was treated with dox (1µg/ml) for 0, 3, 5, and 11 days before harvesting. ChIP and MeDIP were performed using LowCell# ChIP and MagMeDIP kits, respectively, with the Bioruptor sonicator (all from Diagenode). For ChIP, we used the following antibodies: anti-H3K27me3 (Milipore, 07-449), anti-H3K9me3 (Abcam, ab8898), anti-acetyl-H3 (Millipore, 06-599), anti-H3K4me3 (Abcam, ab8580). For MeDIP, we used the 5-methylcytidine antibody from the MagMeDIP kit (Diagenode). qPCR was performed using SsoFast EvaGreen Supermix on a CFX96-C1000 Real-Time PCR System (both from Bio-Rad Laboratories). For qPCR primer sequences, see Table S1.

Reported fold-enrichment values from qPCR experiments used a standard $\Delta\Delta C_t$ method. Here, we denote the threshold cycle number for amplification of a given locus in an experiment involving chromatin regulator CR as $C_t(locus, CR)$. In a first step, we normalized by an internal positive control locus for that particular modification, denoted $C_t(control, CR)$ (see below for choice of control locus for each modification). Second, we normalized this value by the ΔC_t between the locus of interest and the control locus in the parental cell line without any CR:

$$fold - change = \frac{2^{\{C_t(locus,CR) - C_t(control,CR)\}}}{2^{\{C_t(locus,parental) - C_t(control,parental)\}}}$$

The internal control loci account for variations in the amount of DNA and pull-down efficiency for each sample. For this purpose we selected β-actin for the marks associated with active genes (H3K4me3 and histone acetylation) and Igf2 for the silencing marks (H3K27me3, H3K9me3, and 5mC). Igf2 was chosen for its lack of expression in mouse adult ovary cells (MGI Ref. ID J:46439) and elevated levels of H3K9me3 and H3K27me3 implicated in the imprinting of the locus (*39*).

Flow cytometry for epigenetic memory analysis

For each cell line, cells were plated in multiple wells at the same time, and either treated with dox (1 μg/ml) starting at different times (1, 2, 3, and 5 days before dox removal), or grown in the absence of dox (for background silencing correction). Dox was removed simultaneously from all samples. At different time points following dox removal, cells were harvested using 0.25% Trypsin (Life Technologies). A fraction of the cells (varying between one half to one tenth, depending on cell density) were re-plated for the next time point. The rest of the cells were resuspended in flow buffer (Hank's Balanced Salt Solution (Life Technology) and 2.5 mg/ml BSA), and filtered through 40 μm strainers (BD Falcon) to remove clumps. Cellular fluorescence distributions were measured with a MACSQuant VYB flow cytometer (Miltenyi Biotec, Bergisch Gladbach, Germany). The resulting data were analyzed with a custom Matlab program called EasyFlow (available upon request). Single cells were selected based on side and forward scatter properties, and only mCherry-expressing cells were analyzed. A manual gate was imposed on the Citrine fluorescence to determine the percent of silent cells for each sample (Fig. 2C and S7A-C). The gate was selected to contain 1-2% of the positive Citrine peak of untreated cells.

Background silencing correction for long-term experiments

In all cell lines containing CRs, we noticed an increase in the percentage of silent cells over 30 days, even in the absence of dox treatment (Fig. S7D). This background silencing is a combination of spontaneous silencing of the reporter locus (as seen in the parental line with no CRs, Fig. S7D), and non-specific silencing of the reporter by each rTet-CR fusion in the absence of dox (likely by dox-independent binding of rTetR to DNA). In order to correct for this background silencing, for each cell line, we subtracted the fraction of cells silenced in the untreated line and normalized by the fraction of untreated cells that were active at each time point. This allowed us to obtain the fraction of cells that were silenced specifically by CR recruitment:

$$C_S(background\ corrected) = \frac{C_S(dox\ treated) - C_S(untreated)}{C_A(untreated)},$$

where $C_S(dox\ treated)$ and $C_S(untreated)$ are the fraction of cells silenced in the dox treated and untreated samples, respectively, and $C_A(untreated)$ is the fraction of cells active in the untreated sample at the same time point.

Extracting the transition rates

During EED and KRAB recruitment, using the model presented in Fig. 3A (upper panel), with an initial condition in which all cells are active, the exact solutions for the time evolution of the fraction of cells active (C_A), reversibly silent (C_R), and irreversibly silent (C_I) are:

$$C_A(t) = \frac{1}{\gamma_2 - \gamma_1}[(k_A + k_I - \gamma_1)e^{-\gamma_1 t} - (k_A + k_I - \gamma_2)e^{-\gamma_2 t}]$$

$$C_R(t) = \frac{k_S}{\gamma_2 - \gamma_1}[e^{-\gamma_1 t} - e^{-\gamma_2 t}] \qquad \text{(Eq. 1)}$$

$$C_I(t) = [1 - \frac{k_S k_I}{\gamma_1(\gamma_2 - \gamma_1)}e^{-\gamma_1 t} + \frac{k_S k_I}{\gamma_2(\gamma_2 - \gamma_1)}e^{-\gamma_2 t}]$$

where k_S, k_A, and k_I are the rates of silencing, reactivation, and irreversible commitment, respectively. We have also defined:

$$\gamma_1 = \frac{k_S + k_A + k_I - \sqrt{(k_S + k_A + k_I)^2 - 4k_S k_I}}{2},\ \gamma_2 = \frac{k_S + k_A + k_I + \sqrt{(k_S + k_A + k_I)^2 - 4k_S k_I}}{2}.$$

Note that the total fraction of cells silent is the sum of cells that are reversibly and irreversibly silent: $C_S(t) = C_R(t) + C_I(t)$.

Additionally, during recruitment, we experimentally observed a time lag between dox addition and the onset of silencing, which we denote T_{lag_1}. Therefore, for fitting purposes, in the equations above, t becomes $t - T_{lag\_1}$ for recruitment times larger than T_{lag_1}. We assume the fractions of silent/active cells are constant before T_{lag_1}.

During EED and KRAB release, we assume that the rates of silencing and irreversible commitment are negligible (Fig. 3A, lower panel). This means that the fraction of cells silent after CR release (dots in Fig. 3C-F) decays exponentially at a constant rate (k_A). More specifically, defining $C_S(t, \tau)$ as the fraction of cells silenced after a recruitment period of duration t, and release time τ, we have:

$$C_S(t, \tau) = C_R(t) \cdot e^{-k_A(\tau - T_{lag\_2})} + C_I(t) \qquad \text{(Eq. 2)}$$

where $C_R(t)$ and $C_I(t)$ are the fraction of cells in the R and I states, respectively, at the end of recruitment, and T_{lag_2} is the time lag before reactivation starts.

For EED and KRAB, the silencing and reactivation data at a given dox concentration were fit simultaneously using Equations 1 and 2 for silencing and reactivation phases, respectively. For maximum dox (1000 ng/ml), these data consist of the fraction of cells silent during recruitment (Fig. 1H), and the fraction of cells silent during release for all durations of recruitment (Fig. 3C-F). We use the "fit" function in MATLAB to perform a

nonlinear least square fit with two independent parameters, t and τ, in order to extract k_S, k_A , k_I, k_A , T_{lag_1} and T_{lag_2}. The fits are shown as solid lines in Fig. 3C-F and Fig. S9B-E. The values of the fitted parameters and their 95% confidence intervals for each dox concentration are plotted in Fig. 3G-I.

Note that during silencing at maximum recruitment strength, the rate of silencing (k_S) is much higher than the rates of reactivation (k_A) and irreversible commitment (k_I). Therefore, the fraction of silent cells over time during recruitment (dots in Fig. 1H) can be well-described using an exponential function that only depends on the rate of silencing (k_S):

$$C_S(t) = \begin{cases} 0 & \text{, for } t < T_{lag\_1} \\ 1 - e^{-k_S(t - T_{lag\_1})} & \text{, for } t \geq T_{lag\_1} \end{cases},$$

where t is the recruitment duration, and T_{lag_1} is the time lag before the onset of silencing. The resulting fits using this approximation are plotted as solid lines in Fig. 1H.

During HDAC4 recruitment, the fraction of cells silent as a function of recruitment time is equal to the fraction of cells reversibly silent, since there is no irreversibly silent state:

$$C_S(t) = C_R(t) = \begin{cases} 0 & \text{,for } t < T_{lag\_1} \\ \frac{k_S}{k_S + k_A}\left(1 - e^{-(k_S + k_A)(t - T_{lag\_1})}\right) & \text{,for } t \geq T_{lag\_1} \end{cases}, \qquad \text{(Eq. 3)}$$

During reactivation, for HDAC4, all cells that were reversibly silenced at the end of the recruitment period (t) reactivate at a constant rate (k_A):

$$C_S(t, \tau) = C_R(t) \cdot e^{-k_A \tau} \qquad \text{(Eq. 4)}$$

The fraction of cells silent during recruitment and after release of HDAC4 were fit simultaneously with Equations 3 and 4 using nonlinear least square fitting in MATLAB to extract k_S, k_A , T_{lag_1}, and their 95% confidence intervals.

For DNMT3B, the fraction of cells silent during recruitment is equal to the fraction of cells irreversibly silent (since we assume there is no reversible state), and increases with time as follows:

$$\mathrm{C_S(t)} = \mathrm{C_I(t)} = \begin{cases} 0 & \text{,for t} < \mathrm{T_{lag\_1}} \\ 1 - \mathrm{e}^{-\mathrm{k_I(t - T_{lag\_1})}} & \text{,for t} \geq \mathrm{T_{lag\_1}} \end{cases}, \qquad \text{(Eq. 5)}$$

During release, the fraction of cells irreversibly silent is constant across all times post-dox (τ), and only depends on the duration of recruitment, t:

$$\mathrm{C_S(t, \tau) = C_I(t)} \qquad \text{(Eq. 6)}$$

As with the other CRs, for DNMT3B we simultaneously fit the silencing and memory data with Equations 5 and 6 to determine a single k_I and T_{lag_1}, along with 95% confidence intervals.

At non-saturating dox concentration, for EED and DNMT3B, which silence slowly, the fraction of cells silenced during recruitment was measured only by flow cytometry. For KRAB and HDAC4, which silence fast, the fraction of cells silenced during recruitment at non-saturating dox concentrations were measured using time-lapse microscopy, as in Fig. 1.

Supplementary Text

Connection between molecular and operational models of chromatin-mediated gene silencing and reactivation

The three-state model (Fig. 3A) represents an operational view of chromatin-mediated gene expression dynamics that is different from, and complementary to, molecular models of chromatin regulation, in which stochastic writing, spreading and erasing of chromatin modifications lead to expansion and shrinkage of chromatin domains (*9*, *40*). Here, we ask whether the silencing and reactivation dynamics observed here are consistent with a previous model of chromatin spreading dynamics (*9*). To do so, we expand the chromatin spreading model described by Hathaway et al (*9*), by adding a direct connection between chromatin state and gene expression.

In both the model in (*9*), and our expanded model, the chromatin is represented by an array of nucleosomes that can each be in one of two states: modified and unmodified (Fig. S10). The dynamics are controlled by three reactions: (1) Nucleation: CR recruitment leads to modification of the central nucleosome of the array at a rate k_+. (2) Spreading: Modifications can stochastically spread to neighboring nucleosomes at the same rate k_+, both in the presence or absence of the CR. (3) Loss: Modifications can be lost from any modified nucleosome at a constant rate k_-. The rates k_+ and k_- were previously estimated for HP1 recruitment to be 0.176 h^{-1} and 0.117 h^{-1}, respectively (*9*, *40*). Here we choose a nucleosome array length of 51 nucleosomes. This size is beyond the average size of experimentally observed domains (*9*), and big enough to allow the simulated domain to spread without boundary effects. Further increase in array size does not affect dynamics for the parameters used here.

To connect this existing chromatin spreading model with gene regulation dynamics, we next added an arbitrary threshold, which determines the minimum size of the chromatin modification domain in the immediate neighborhood of the promoter required for a gene to be silenced. We used a value of 11 nucleosomes for the size of the neighborhood, and considered the gene to be silent when at least 4 of these 11 nucleosomes are modified. Otherwise it was assumed to be active (Fig. S10B). This particular threshold was chosen such that >80% of cells are silenced by 5 days, and reactivate within 30 days, consistent with EED dynamics here, and with HP1 dynamics reported in ref. (*9*).

Simulations of the model described above show stochastic silencing and reactivation. The fraction of silent cells as a function of time during recruitment and release can be well-fit by the three-state model described in Fig. 3A, with constant rates $k_S, k_A,$ and k_I (Fig. S10C and D). These results show that, with a simple assumption about the connection between the domain size of a modified region and gene expression, the spreading model can give rise to the three-state dynamics described in the text. However, we note that it currently remains unclear whether silencing dynamics are in fact dominated by chromatin modifications spreading.

Connection between all-or-none and graded modes of gene expression regulation

All-or-none stochastic switching of gene expression states can occur at two levels: In this paper, we focus on transitions between active and silent chromatin states. However, even within an active chromatin state, promoters in general switch stochastically between transcriptionally active and inactive states (this phenomenon is called transcriptional bursting; see (*41*) for a review). Here we discuss the connection between these two modes of gene regulation and analyze the dynamic regimes that lead to either graded or fractional all-or-none responses at the protein level. Using stochastic simulation, we also show that chromatin-mediated switching generally produces bimodal protein distributions similar to those observed experimentally, but can also produce graded protein level distributions in some parameter regimes.

The two levels of gene regulation, chromatin-mediated switching and transcriptional bursting, can be combined in a single model (Fig S11A) (*41*). In this model, a gene can switch between active and silent chromatin states. In the silent chromatin state, the promoter is always inactive, so the level of mRNA production is zero. By contrast, the active chromatin state is permissive, allowing the promoter to switch between periods of active transcription, which produce bursts of multiple mRNA molecules, and periods of inactivity (*42–44*).

Transitions in chromatin state and transcriptional bursting are associated with different timescales. At the transcription level, switching between active and inactive promoter states (indicated with rates k_{off} and k_{on} in Fig. S11A) has been attributed to short-lived interactions of transcription factors and core machinery with the promoter, occurring on the timescale of seconds to minutes (*41*). At the chromatin level, our data suggest that switching between active and silent chromatin states (indicated with k_S and k_A, Fig. 3A and Fig. S11A) occur on the timescale of hours to days, an order of magnitude slower than the timescales involved in transcriptional bursting.

The timescales of switching can determine the distribution of protein levels at the population level. When switching timescales are fast relative to mRNA and protein half-lives, which is typically the case for transcription factor regulation, the level of protein expressed from the gene reaches a steady state unimodal distribution (*45*). The mean value of this distribution depends in a graded manner on the occupancy of the transcription factor at the promoter (*29*, *31*). When switching timescales are slow relative to mRNA and protein half-lives, as is generally the case for chromatin-mediated regulation, one expects bimodal protein distributions. The relative ratio of the two peaks in this bimodal distribution depends both on the occupancy of the CR at the promoter, and on the time it has been recruited there.

Based on the parameters measured here for CR-mediated silencing, EED, KRAB, and DNMT3B all operate in the slow switching regime that gives rise to bimodal protein distributions across various dox concentrations (Fig. S11B-D). HDAC4 shows all-or-none stochastic silencing at strong recruitment strengths (saturating dox concentrations). However, as dox concentrations are decreased, the protein levels distributions shift in a graded manner (Fig. S11E).

To test if all-or-none silencing and reactivation at the chromatin level alone can recapitulate reporter protein distributions over various CRs and conditions, we performed

stochastic simulations using the combined chromatin and transcription regulation model described in Fig. S11A. For these simulations we used the experimentally measured rates associated with chromatin-mediated gene switching - k_S, k_A, and k_I - for each CR across different dox concentrations (Fig. 3G-I). To simplify the simulation and limit the source of stochastic switching to the chromatin level, we consider the regime in which $k_{on} \gg k_{off}$. Under this approximation, the promoter is always active within the active chromatin state. The mRNA and protein production rates β_m (100 hr^{-1}) and β_p (200 hr^{-1}) are chosen such that the resulting mean H2B-Citrine fluorescence levels in the fully active state (without dox) from simulations match those obtained in flow cytometry experiments. We use the experimentally measured mRNA degradation rate γ_m=0.1733 hr^{-1} (corresponding to a half-live of 4 hours, as shown in Fig. S2B). We assume that the number of molecules for each mRNA and protein species is halved at every cell division (dilution). Since H2B-citrine is stable, we set the protein degradation to zero. Lastly, each simulated cell has its cell cycle length drawn randomly from a normal distribution with mean and variance derived from those empirically observed in movie experiments.

Stochastic simulation of the model in this regime recapitulated bimodal responses of EED, KRAB and DNMT3B (Fig. S11F-H), reflecting the fact the lifetime of the silent state remains longer than the protein and mRNA lifetimes, regardless of dox concentrations. The model also recapitulated the graded response of HDAC4 observed at sub-saturating dox concentrations (Fig. S11I), reflecting the fact that in these conditions k_S and k_A are similar, resulting in lifetimes of the silent state that are on the order of protein dilution (i.e. cell division time). Together, these results demonstrate how a stochastic, all-or-none model of chromatin-mediated silencing and reactivation is sufficient to explain the protein distributions obtained for all four CRs.

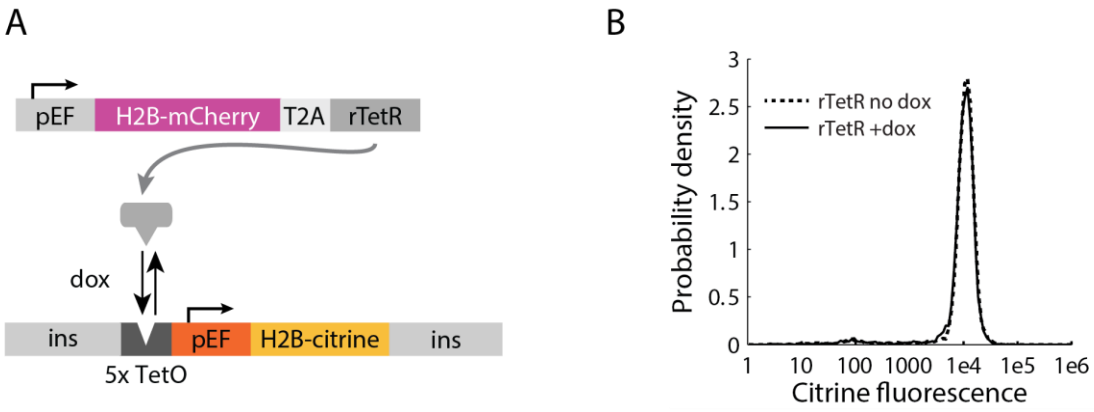

Fig. S1. Recruitment of rTetR alone does not repress gene expression.

To test whether recruitment of rTetR alone (without an attached CR fusion) affects reporter expression, we measured Citrine fluorescence levels in reporter cells stably expressing pEF-H2B-mCherry-T2A-rTetR. **(A)** Schematic of the cell line. **(B)** Flow cytometry shows identical fluorescence distributions in the absence of dox (dashed line) and after 33 hours of dox induction (continuous line), indicating that rTetR recruitment alone does not repress gene expression.

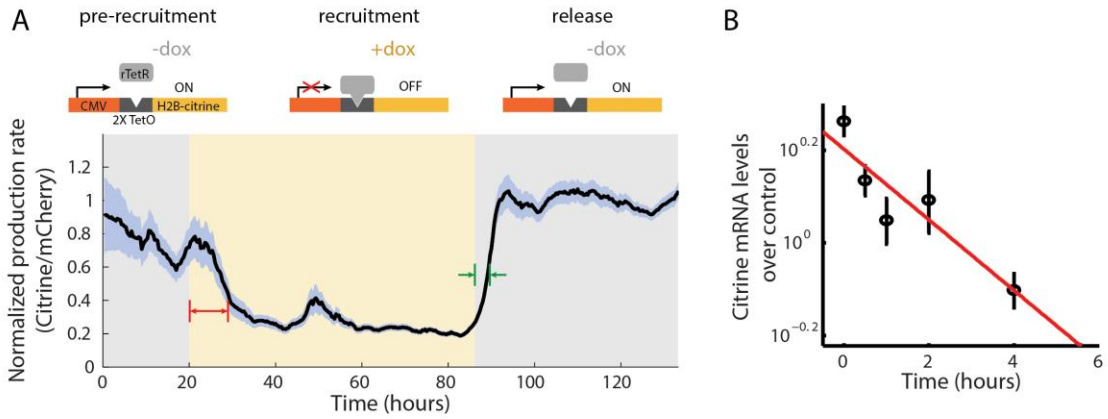

Fig. S2. Timescales for detecting silencing and reactivation events, and reporter mRNA lifetime.

(A) In order to estimate the response time to rTetR recruitment and de-recruitment, we built a separate cell line containing the rTetR domain alone recruited to a CMV promoter followed by 2xTetO sites (top cartoons). In this case, binding of rTetR directly represses expression by acting as a transcription roadblock. We measured changes in reporter production rates using time-lapse microscopy. We calculated the mean Citrine production rate (see Fig. 1C) as a function of time (black curve) by averaging over single-cell traces at each time point. Since cells were dividing, the number of traces analyzed for each time point varied between 62 cells (first time point) to 926 cells (last time point). The gray shaded curves represent SEM. Addition of dox resulted in a reduction in gene expression within 8±2 hours (red arrows). Removal of dox relieved this repression within 2.5±2 hours (green arrows). **(B)** The half-life of Citrine mRNA was measured by inhibiting transcription with actinomycin D (5µg/ml) and following the levels of mRNA as a function of time. These values were measured by qPCR and normalized against a constant amount of mCherry mRNA spiked in as internal control. By fitting these data to an exponential decay (red line), we determined the half-life of the reporter mRNA to be 3.9 hours (with a 95% confidence interval of [0.9, 4.3] hours).

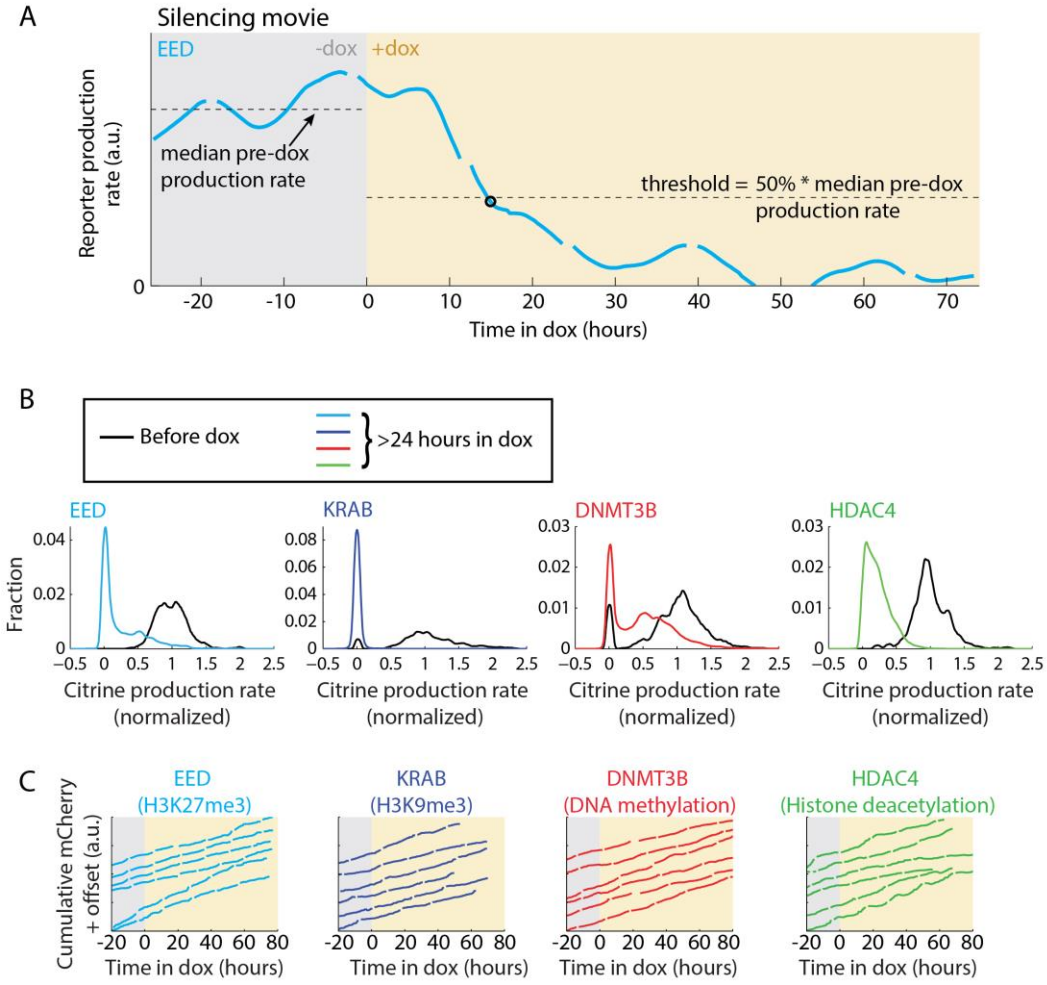

Fig. S3. Event detection, specificity and strength of silencing.

(A) Silencing events were detected by setting a threshold on the reporter production rate, computed as the smoothed time derivative of the cumulative Citrine fluorescence trace (cyan curve, same cell lineage as in Fig. 1C). Note that frames immediately adjacent to cell division events were unreliable and therefore removed when the raw total fluorescence traces were processed to produce cumulative traces, resulting in gaps in the trace. For silencing, we calculated the median reporter production rate before dox addition, and set a threshold at 50% of this value (dashed line in dox region). When the reporter production rate of this lineage crossed this threshold and remained under it for ≥12 hours, we classified the event as silencing (black circle). **(B)** Recruitment lead to strong silencing for all four factors. Distributions of H2B-citrine production rates before dox (black) and after more than 24 hours in dox (colors, each normalized to the corresponding median pre-dox production rate), showing that the production rates in most silenced cells collapse to a peak around zero. **(C)** Single-cell traces in the constitutive reporter H2B-mCherry channel, of the same cell lineages shown in Fig. 1D and arranged in the same order. Traces are vertically offset for clarity. The H2B-mCherry reporter showed steady production in all traces, indicating that dox-mediated silencing is likely specific to the H2B-Citrine reporter locus rather than a genome-wide effect.

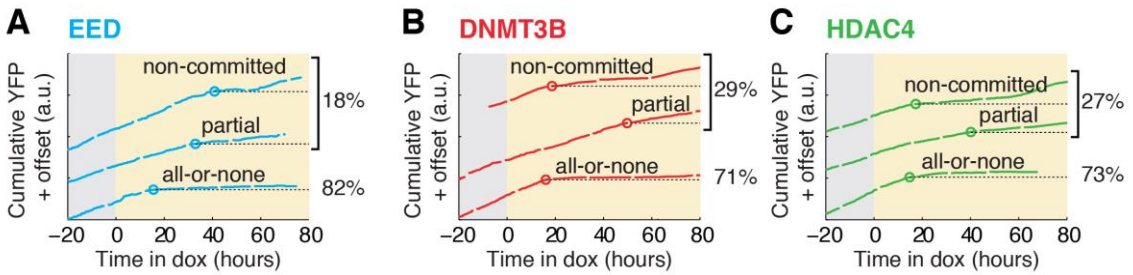

Fig. S4. Deviations from all-or-none silencing dynamics.

Here we plot examples of silencing dynamics that deviated from all-or-none behaviors for **(A)** EED, **(B)** DNMT3B, and **(C)** HDAC4. (For KRAB, we observed no deviations). In each panel, a representative example trace is shown for each of two types of non-typical behaviors, with their observed frequencies indicated by percentages relative to all traces. First, partial silencing events are defined as traces that show reduced but not fully silenced expression. These are defined by a lack of full silencing within 1.5 cell cycles after the initial silencing event (middle trace). Second, non-committed silencing events are those in which a strong silencing event is followed by a subsequent increase in activity (top trace). Circles indicate detected silencing events. For comparison, we also plot examples of typical all-or-none silencing events (bottom traces).

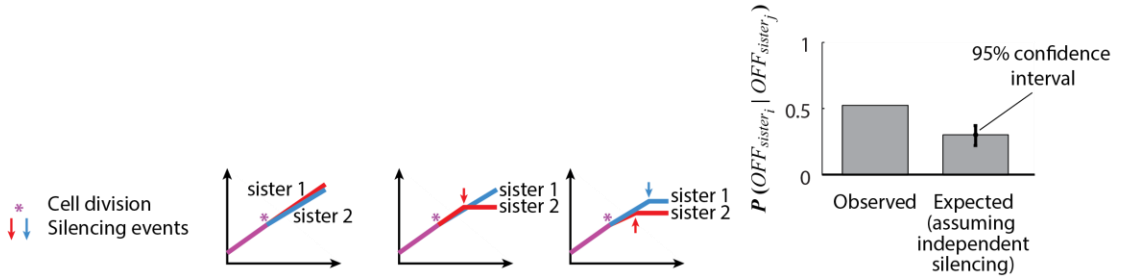

Factor	Number of sister cells pairs (Observed)				Conditional probability of silencing Observed / Expected
	Total	ON/ON	ON/OFF	OFF/OFF	
EED	288	161	82	45	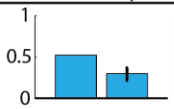
KRAB	34	0	4	30	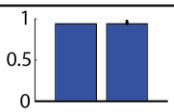
DNMT3B	207	105	75	27	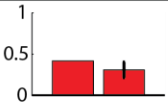
HDAC4	43	5	8	30	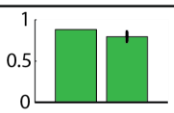

Fig. S5. Analysis of sister cell correlation during silencing.

We tabulated the numbers of sister cell pairs originating from an actively expressing parent cell, and compared their silencing behavior in the first cell cycle after division of the parent cell. For each factor, we measured the number of sister pairs in which both sister cells remained active (ON/ON column), only one sister cell was silenced (ON/OFF column), and both sister cells were silenced (OFF/OFF column). From these observations, we computed the conditional silencing probability of a sister cell given the other sister cell is silenced, i.e., $P\left(OFF_{sister_i} \middle| OFF_{sister_j}\right) = \frac{2 * OFF/OFF}{2 * OFF/OFF + ON/OFF}$, see last column, left bars. We compared this observed conditional silencing probability to the expected counterpart, assuming silencing events are stochastic and independent in the two sisters. This expected probability and its 95% confidence intervals (last column, right bars) were estimated using the same equation on results from a random permutation test with 100,000 trials. Note that while the observed probability is higher than the expected value for EED, DNMT3B and HDAC4, these observed values were still closer to the expected values assuming complete independence, than to the expected value assuming complete correlation (P = 1), or complete anti-correlation (P = 0) between sister cells. These results suggest a substantial stochastic component in the silencing process.

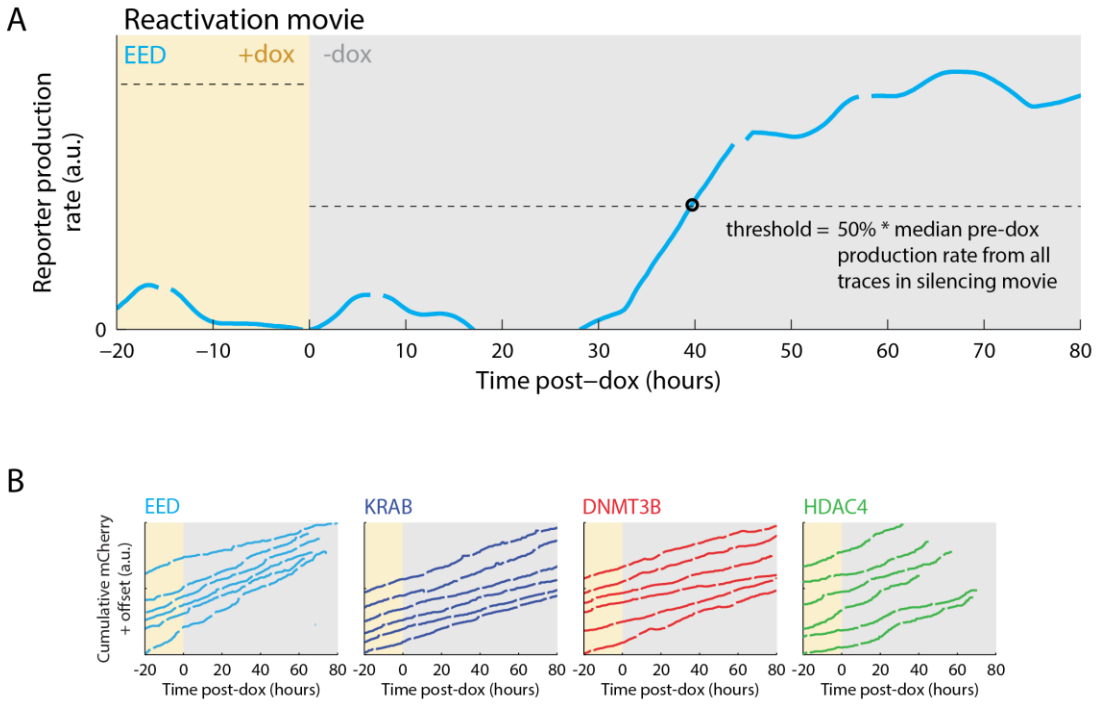

Fig. S6. Detection of reactivation events.

(A) The cyan curve is the smoothed time derivative of the cumulative fluorescence trace for the same lineage shown in Fig. 2A. Reactivation events were detected in a similar way as silencing events, but in the opposite direction. The median pre-dox production rate from all lineage traces in the silencing movie (Fig. 1) immediately preceding the reactivation movie was used to set a single threshold to detect reactivation events (dashed line). Reactivation events were defined by an increase in production rate above this threshold that was sustained for ≥12 hours. **(B)** Single-cell traces of the constitutive reporter H2B-mCherry channel, of the same cell lineages shown and arranged as in Fig. 2B, show steady production rates, indicating that reactivation is specific to the H2B-Citrine reporter locus. Traces are offset for clarity.

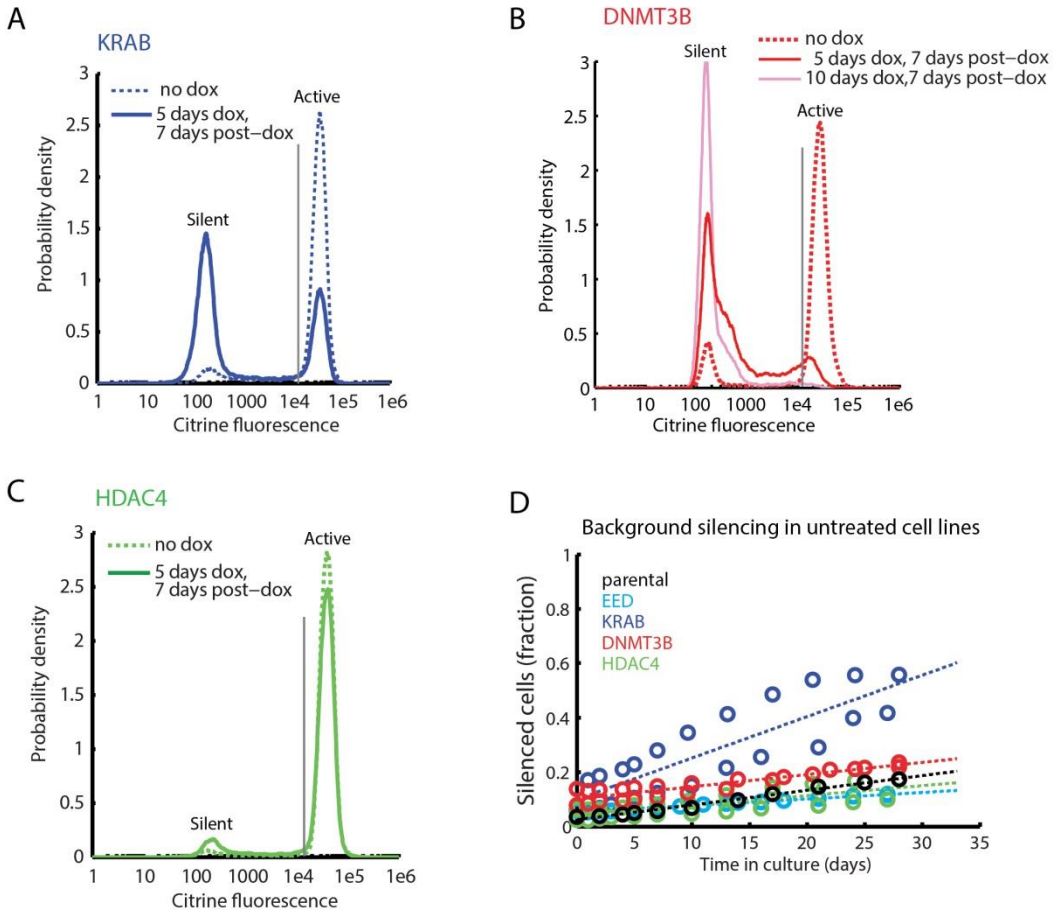

Fig. S7. Bimodality during reactivation.

(A to C) Citrine fluorescence distributions as measured by flow cytometry for the **(A)** KRAB, **(B)** DNMT3B, or **(C)** HDAC4 cell lines. These plots are comparable to that of EED in Fig. 2C. For all CRs, distributions are shown for cells treated with dox for 5 days, followed by 7 days of culture without dox (solid lines, blue, red and green), and for cells cultured in parallel with no dox (dashed lines). Note that for DNMT3B, the fluorescence distribution after 5 days of dox and 7 days post-dox deviates slightly from a bimodal distribution: the silent population has a small sub-population with fluorescence above background levels (shoulder in red continuous line). The percentage of cells in this outlier subpopulation decreases with longer recruitment times, as seen in the curve for 10 days of dox treatment (pink). The vertical gray line in each panel represents the threshold used to determine the fraction of cells silent. **(D)** Low rates of background silencing occur even in the absence of dox evident as an increase in the fraction of silent cells over time in untreated samples (see silent peak of no dox (dotted) lines in A-C). Data from two independent biological replicates are shown for each CR. To correct for this background silencing effect, we subtracted the fraction of cells silenced in the absence of dox from the fraction of cells silenced with dox addition, to generate the plots in Figs. 2D, 3C-F, and S9B-E. For each data point we used a corresponding control (no dox background) measured on the same day. See Materials and Methods for more details.

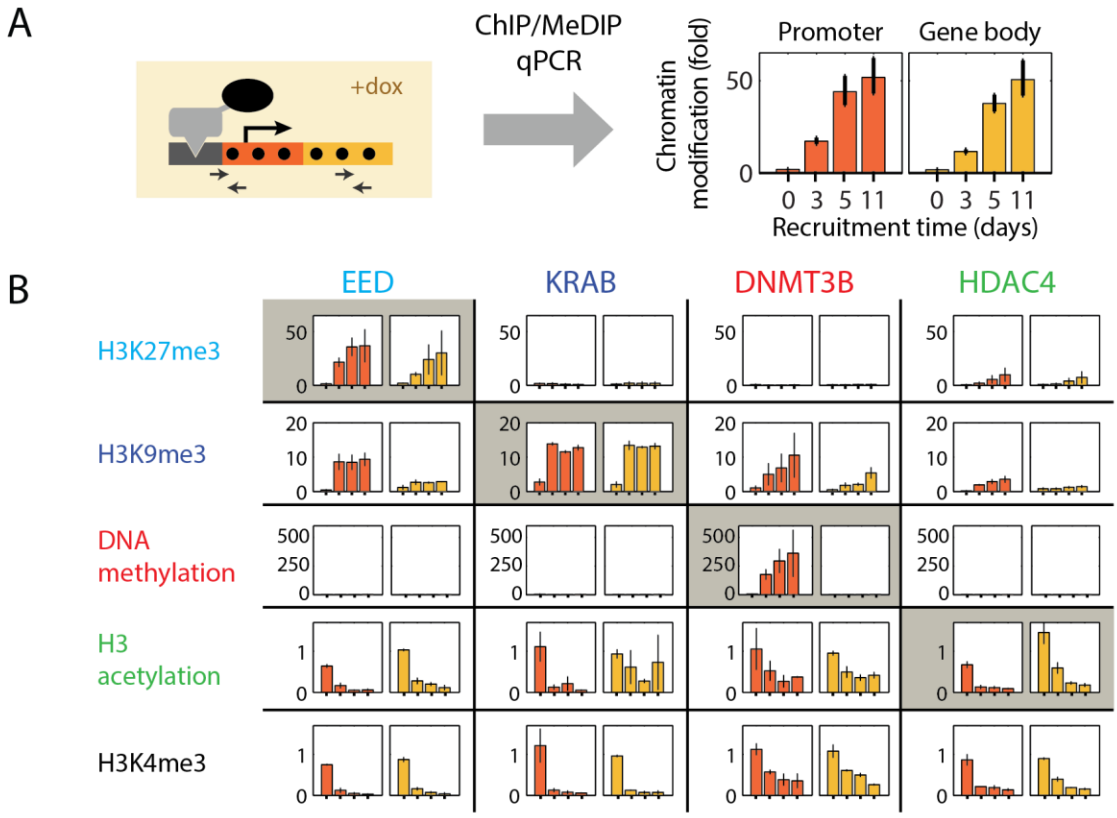

Fig. S8. Chromatin regulators produce molecularly distinct silent states.

(A) Experimental strategy: We used chromatin immunoprecipitation (ChIP) and methyl-DNA immunoprecipitation (MeDIP), followed by qPCR to quantify five common chromatin modifications, at the promoter (orange, arrows) and in the gene body (yellow, arrows), after different durations of CR recruitment: 0, 3, 5 or 11 days of dox treatment (Materials and Methods). qPCR signals were normalized by β-Actin (for active marks) or Igf2 (for repressive marks) and plotted as fold-change (mean ± s.d.) relative to the parental (reporter only) cell line. **(B)** Matrix showing how each chromatin regulator affected the levels of each modification, following the conventions from (A). As expected, each CR promoted its corresponding modification (shaded plots). Additionally, recruitment of one CR also led, directly or indirectly, to other modifications: active modifications (H3 acetylation and H3K4me3) decreased in all cases, and the repressive H3K9me3 modification associated with KRAB also appeared in response to EED and DNMT3B recruitment, consistent with previous reports (*46–49*). By contrast, H3K27me3 and DNA methylation were more specific to EED and DNMT3B, respectively. As a result, although the molecular states produced by individual CRs partially overlapped, each CR produced a silent state with a distinct molecular signature (each column is unique).

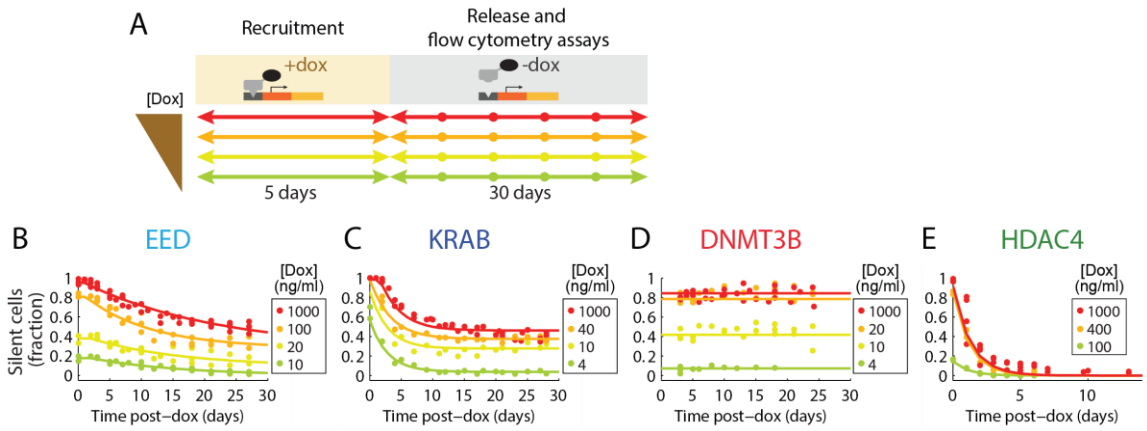

Fig. S9. Different CRs maintain their distinct dynamic modes at lower recruitment strengths.

(A) Experimental design: For each CR, cells were induced for 5 days at varying dox concentrations (different color arrows, with dox concentrations increasing from green to red). The fraction of silent cells was measured by flow cytometry for 30 days following CR release (post-dox). **(B-E)** Examples of reactivation dynamics after recruitment at different dox concentrations. The fraction of cells that remain silent after CR release is plotted against the time since dox was removed. Dots represent experimental data from at least two independent sets of flow cytometry experiments, and lines are fits to these data with the models as in Fig. 3C-F. For each CR, the strength of recruitment (i.e. dox concentration) controls the fraction of silent cells in a similar manner to the duration of recruitment (compare to Fig. 3C-F). Even at lower recruitment strength, EED and KRAB show hybrid memory, DNMT3B leads to irreversible silencing, and HDAC4 produces reversible silencing.

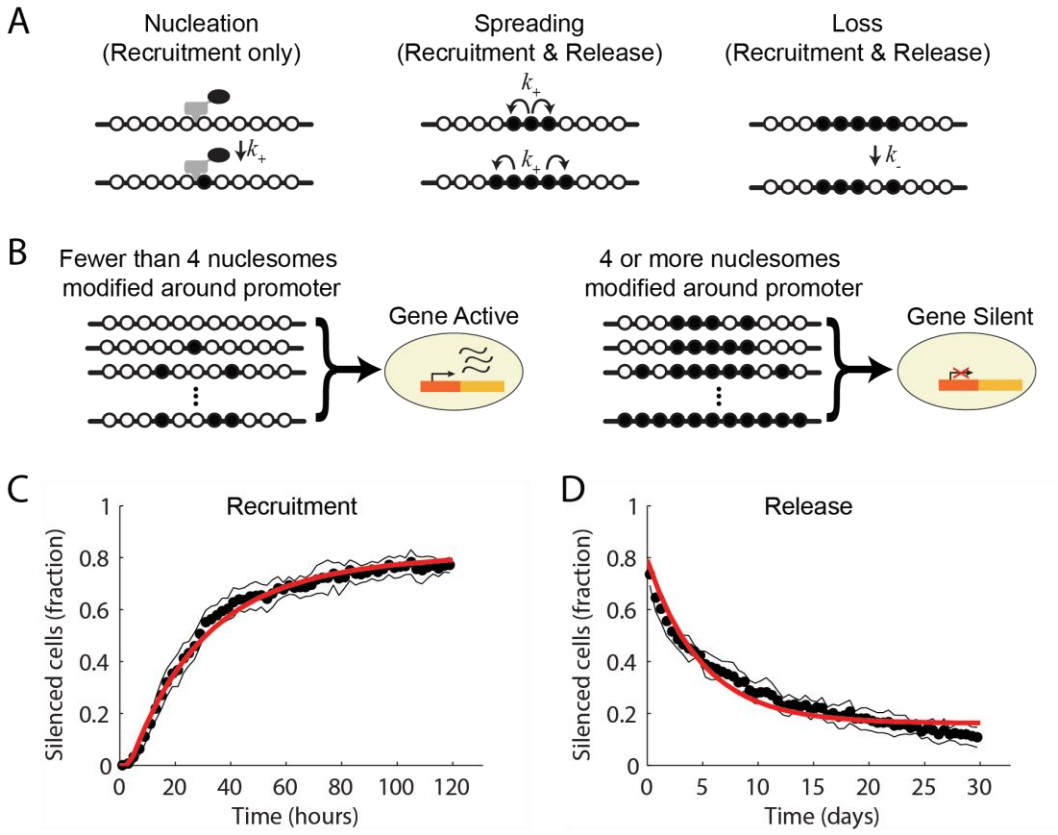

Fig. S10. Spreading of chromatin modifications can lead to stochastic silencing and reactivation at constant rates.

(A) Molecular model of chromatin modifications dynamics, adapted from (*9*). An array of nucleosomes (circles) that can each be in one of two states: unmodified (white), and modified (black). Upon recruitment of a CR, the target nucleosome at the center becomes modified (left), at a rate k_+. Modifications can stochastically spread to the neighboring nucleosomes at the same rate k_+ (middle). These modifications can be lost at a constant rate k_- along the array (right). In the simulation, nucleation takes place only during recruitment of a CR, while spreading and loss happen both during recruitment and release of the CR. **(B)** In order to connect chromatin states to gene expression, we set an arbitrary threshold: during the simulation, the gene is considered silent if 4 or more of the 11 nucleosomes closest to the target site are modified (left), and active otherwise (right). **(C, D)** The fraction of cells silenced as a function of time during CR recruitment (C) and release (D) obtained from a molecular simulation using the model described in (A) and (B) are shown in black. For the simulation we used the gain/spreading and loss rates estimated in (*9*): k_+=0.176 h^{-1} and k_-=0.117 h^{-1}. Black dots represent the average for 100 cells/arrays, and the black lines represent standard deviations over 10 trials. These simulated data can be fit by the three-state model shown in Fig. 3A (red lines), with the following rates: $k_S = 0.7\,d^{-1}$, $k_A = 0.2\,d^{-1}$, $k_I = 0.06\,d^{-1}$, and lag times before silencing $T_{lag\_1} = 0.15\,d$, and before reactivation $T_{lag\_2} = 0\,d$. These rates are comparable to the ones we measure for EED and KRAB silencing and reactivation from experimental results.

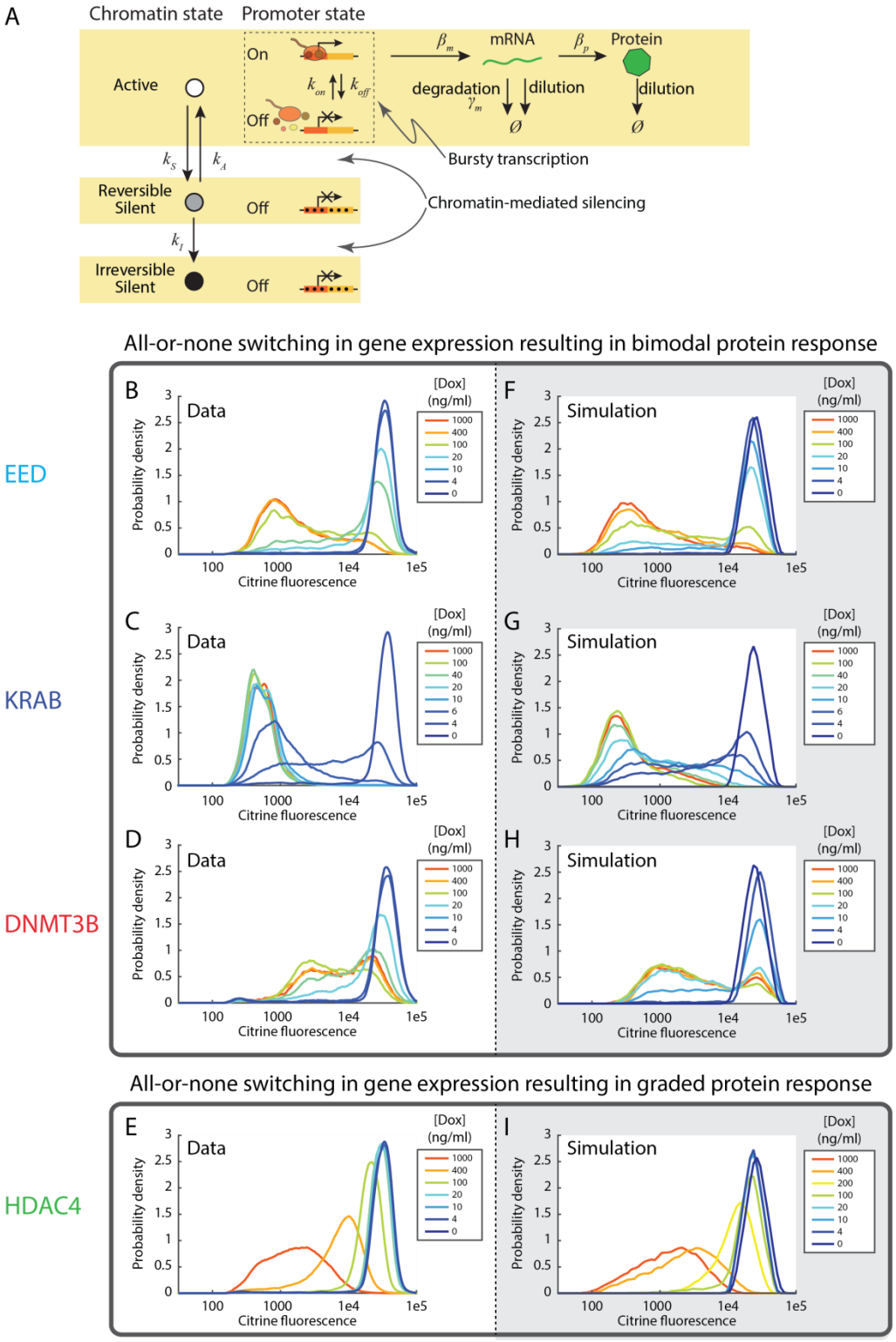

Fig. S11. All-or-none silencing and reactivation can lead to bimodal or graded protein distributions that resemble those observed experimentally.

(A) The three-state chromatin model can be combined with a stochastic transcription model by incorporating additional gene expression steps (see "Connection between all-

or-none and graded modes of gene expression regulation" in Supplementary Text). **(B to E)** Citrine fluorescence distribution as measured by flow cytometry for (B) EED, (C) KRAB, (D) DNMT3B, or (E) HDAC4 cell lines. Cells were treated at the indicated dox concentrations for five days before measurement, and no release time was allowed (unlike the conditions in Fig. S7). Note that in this case the slow dilution of stable reporter protein contributes significantly to the observation of intermediate protein levels in bimodal distributions. **(F to I)** Fluorescence distribution of cell populations for (F) EED, (G) KRAB, (H) DNMT3B, or (I) HDAC4, simulated using the model in (A) and experimentally derived parameters (Fig. 3G-I).

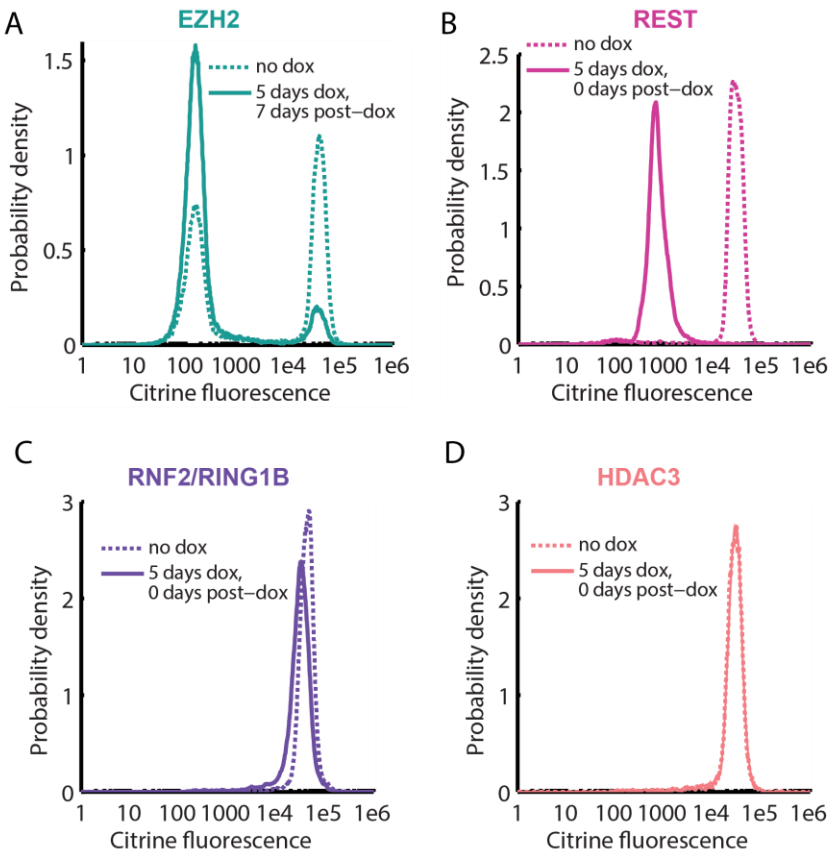

Fig. S12. Silencing by other CRs.

Cells containing different rTetR-CR fusions were induced by dox treatment for 5 days, and their fluorescent distributions were measured using flow cytometry. We observed bimodal silencing for **(A)** EZH2 and **(B)** REST. We observed very little or no silencing for **(C)** RNF2/RING1B and **(D)** HDAC3, respectively.

Table S1. Primers used for ChIP-qPCR and MeDIP-qPCR

Locus	Name	Sequence
pEF (promoter)	pEF_F_1013ChIP	ACGTATGTCGAGGTAGGCGT
	pEF_R_1013ChIP	CTAGGCACCGGTTCAATTGC
citrine (gene body)	F_cit_Set2	CGGCGACGTAAACGGCCACAAGTTCAG
	R_cit_Set2	CTTGCCGGTGGTGCAGATGAA
actin (control)	bActin F	ACTGGGACGATATGGAGAAG
	bActin R	GGTCATCTTTTCACGGTTGG
Igf2 (control)	5-42_Igf2_F	CTGTGGCCTGTAGGTCCTTG
	5-43_Igf2_R	CCTCTGCCTTTCCCTCTTGG

Movie S1. Highlighted silencing movie for EED; related to movie S5

Movie S2. Highlighted silencing movie for KRAB; related to movie S6

Movie S3. Highlighted silencing movie for DNMT3B; related to movie S7

Movie S4. Highlighted silencing movie for HDAC4; related to movie S8

Movie S9. Highlighted reactivation movie for EED; related to movie S13

Movie S10. Highlighted reactivation movie for KRAB; related to movie S14

Movie S11. Highlighted reactivation movie for DNMT3B; related to movie S15

Movie S12. Highlighted reactivation movie for HDAC4; related to movie S16

Movies S1-S4 and S9-S12 are zoomed-in views of silencing and reactivation respectively, one for each CR. Each movie is digitally cropped and centered on the specific cells highlighted in Fig. 1C and 2C (for EED) and on one of the lineages shown in Fig. 1D and 2D (for all other factors). Citrine fluorescence is pseudo-colored as yellow. All cells segmented (using mCherry fluorescence) are circled in red. We focus on one lineage over time by highlighting it with a cyan contour. Only one daughter cell is highlighted after each cell division event. Time stamps are in HH:MM relative to dox addition (for S1 to S4) or dox removal (for S9 to S12). For the highlighted cells, silencing (in S1 to S4) and reactivation events (in S9 to S12) are indicated with thick green circles around the focused cells in the few frames at and following the events. See Movies S5 to S8 and S13 to S16 for dual-channel, un-cropped versions of these movies.

Movie S5. Full silencing movie for EED;

Movie S6. Full silencing movie for KRAB;

Movie S7. Full silencing movie for DNMT3B;

Movie S8. Full silencing movie for HDAC4;

Movie S13. Full reactivation movie for EED;

Movie S14. Full reactivation movie for KRAB;

Movie S15. Full reactivation movie for DNMT3B;

Movie S16. Full reactivation movie for HDAC4;

Movies S5-S8 and S13-S16 are representative, full silencing and reactivation movies for each of the CRs tested. Citrine and mCherry channels are psuedo-colored as yellow and magenta, respectively. Time stamps are relative to dox addition (for S5 to S8) or dox removal (for S13 to S16).

References and Notes

1. T. Kouzarides, Chromatin modifications and their function. *Cell* **128**, 693–705 (2007). Medline doi:10.1016/j.cell.2007.02.005

2. E. Li, Y. Zhang, DNA methylation in mammals. *Cold Spring Harb. Perspect. Biol.* **6**, a019133 (2014). Medline doi:10.1101/cshperspect.a019133

3. V. W. Zhou, A. Goren, B. E. Bernstein, Charting histone modifications and the functional organization of mammalian genomes. *Nat. Rev. Genet.* **12**, 7–18 (2011). Medline doi:10.1038/nrg2905

4. A. Bird, DNA methylation patterns and epigenetic memory. *Genes Dev.* **16**, 6–21 (2002). Medline doi:10.1101/gad.947102

5. J. Zhu, M. Adli, J. Y. Zou, G. Verstappen, M. Coyne, X. Zhang, T. Durham, M. Miri, V. Deshpande, P. L. De Jager, D. A. Bennett, J. A. Houmard, D. M. Muoio, T. T. Onder, R. Camahort, C. A. Cowan, A. Meissner, C. B. Epstein, N. Shoresh, B. E. Bernstein, Genome-wide chromatin state transitions associated with developmental and environmental cues. *Cell* **152**, 642–654 (2013). Medline doi:10.1016/j.cell.2012.12.033

6. M. F. Fraga, M. Esteller, Epigenetics and aging: The targets and the marks. *Trends Genet.* **23**, 413–418 (2007). Medline doi:10.1016/j.tig.2007.05.008

7. G. Egger, G. Liang, A. Aparicio, P. A. Jones, Epigenetics in human disease and prospects for epigenetic therapy. *Nature* **429**, 457–463 (2004). Medline doi:10.1038/nature02625

8. A. J. Keung, J. K. Joung, A. S. Khalil, J. J. Collins, Chromatin regulation at the frontier of synthetic biology. *Nat. Rev. Genet.* **16**, 159–171 (2015). Medline doi:10.1038/nrg3900

9. N. A. Hathaway, O. Bell, C. Hodges, E. L. Miller, D. S. Neel, G. R. Crabtree, Dynamics and memory of heterochromatin in living cells. *Cell* **149**, 1447–1460 (2012). Medline doi:10.1016/j.cell.2012.03.052

10. L. A. Gilbert, M. H. Larson, L. Morsut, Z. Liu, G. A. Brar, S. E. Torres, N. Stern-Ginossar, O. Brandman, E. H. Whitehead, J. A. Doudna, W. A. Lim, J. S. Weissman, L. S. Qi, CRISPR-mediated modular RNA-guided regulation of transcription in eukaryotes. *Cell* **154**, 442–451 (2013). Medline doi:10.1016/j.cell.2013.06.044

11. A. J. Keung, C. J. Bashor, S. Kiriakov, J. J. Collins, A. S. Khalil, Using targeted chromatin regulators to engineer combinatorial and spatial transcriptional regulation. *Cell* **158**, 110–120 (2014). Medline doi:10.1016/j.cell.2014.04.047

12. M. L. Maeder, J. F. Angstman, M. E. Richardson, S. J. Linder, V. M. Cascio, S. Q. Tsai, Q. H. Ho, J. D. Sander, D. Reyon, B. E. Bernstein, J. F. Costello, M. F. Wilkinson, J. K. Joung, Targeted DNA demethylation and activation of endogenous genes using programmable TALE-TET1 fusion proteins. *Nat. Biotechnol.* **31**, 1137–1142 (2013). Medline doi:10.1038/nbt.2726

13. J. C. W. Locke, M. B. Elowitz, Using movies to analyse gene circuit dynamics in single cells. *Nat. Rev. Microbiol.* **7**, 383–392 (2009). Medline doi:10.1038/nrmicro2056

14. S. Urlinger, U. Baron, M. Thellmann, M. T. Hasan, H. Bujard, W. Hillen, Exploring the sequence space for tetracycline-dependent transcriptional activators: Novel mutations

yield expanded range and sensitivity. *Proc. Natl. Acad. Sci. U.S.A.* **97**, 7963–7968 (2000). Medline doi:10.1073/pnas.130192197

15. T. M. Yusufzai, G. Felsenfeld, The 5′-HS4 chicken β-globin insulator is a CTCF-dependent nuclear matrix-associated element. *Proc. Natl. Acad. Sci. U.S.A.* **101**, 8620–8624 (2004). Medline doi:10.1073/pnas.0402938101

16. S. Yamaguchi, Y. Kazuki, Y. Nakayama, E. Nanba, M. Oshimura, T. Ohbayashi, A method for producing transgenic cells using a multi-integrase system on a human artificial chromosome vector. *PLOS ONE* **6**, e17267 (2011). Medline doi:10.1371/journal.pone.0017267

17. R. Margueron, D. Reinberg, The Polycomb complex PRC2 and its mark in life. *Nature* **469**, 343–349 (2011). Medline doi:10.1038/nature09784

18. R. Urrutia, KRAB-containing zinc-finger repressor proteins. *Genome Biol.* **4**, 231 (2003). Medline doi:10.1186/gb-2003-4-10-231

19. K. Ayyanathan, M. S. Lechner, P. Bell, G. G. Maul, D. C. Schultz, Y. Yamada, K. Tanaka, K. Torigoe, F. J. Rauscher III, Regulated recruitment of HP1 to a euchromatic gene induces mitotically heritable, epigenetic gene silencing: A mammalian cell culture model of gene variegation. *Genes Dev.* **17**, 1855–1869 (2003). Medline doi:10.1101/gad.1102803

20. M. Fussenegger, R. P. Morris, C. Fux, M. Rimann, B. von Stockar, C. J. Thompson, J. E. Bailey, Streptogramin-based gene regulation systems for mammalian cells. *Nat. Biotechnol.* **18**, 1203–1208 (2000). Medline doi:10.1038/81208

21. M. Okano, D. W. Bell, D. A. Haber, E. Li, DNA methyltransferases Dnmt3a and Dnmt3b are essential for de novo methylation and mammalian development. *Cell* **99**, 247–257 (1999). Medline doi:10.1016/S0092-8674(00)81656-6

22. E. A. Miska, C. Karlsson, E. Langley, S. J. Nielsen, J. Pines, T. Kouzarides, HDAC4 deacetylase associates with and represses the MEF2 transcription factor. *EMBO J.* **18**, 5099–5107 (1999). Medline doi:10.1093/emboj/18.18.5099

23. K. H. Hansen, A. P. Bracken, D. Pasini, N. Dietrich, S. S. Gehani, A. Monrad, J. Rappsilber, M. Lerdrup, K. Helin, A model for transmission of the H3K27me3 epigenetic mark. *Nat. Cell Biol.* **10**, 1291–1300 (2008). Medline doi:10.1038/ncb1787

24. N. P. Blackledge, A. M. Farcas, T. Kondo, H. W. King, J. F. McGouran, L. L. Hanssen, S. Ito, S. Cooper, K. Kondo, Y. Koseki, T. Ishikura, H. K. Long, T. W. Sheahan, N. Brockdorff, B. M. Kessler, H. Koseki, R. J. Klose, Variant PRC1 complex-dependent H2A ubiquitylation drives PRC2 recruitment and polycomb domain formation. *Cell* **157**, 1445–1459 (2014). Medline doi:10.1016/j.cell.2014.05.004

25. J. F. Margolin, J. R. Friedman, W. K. Meyer, H. Vissing, H. J. Thiesen, F. J. Rauscher III, Krüppel-associated boxes are potent transcriptional repression domains. *Proc. Natl. Acad. Sci. U.S.A.* **91**, 4509–4513 (1994). Medline doi:10.1073/pnas.91.10.4509

26. H. G. E. Sutherland, M. Kearns, H. D. Morgan, A. P. Headley, C. Morris, D. I. Martin, E. Whitelaw, Reactivation of heritably silenced gene expression in mice. *Mamm. Genome* **11**, 347–355 (2000). Medline doi:10.1007/s003350010066

27. V. Pirrotta, D. S. Gross, Epigenetic silencing mechanisms in budding yeast and fruit fly: Different paths, same destinations. *Mol. Cell* **18**, 395–398 (2005). Medline doi:10.1016/j.molcel.2005.04.013

28. Y. Katan-Khaykovich, K. Struhl, Dynamics of global histone acetylation and deacetylation in vivo: Rapid restoration of normal histone acetylation status upon removal of activators and repressors. *Genes Dev.* **16**, 743–752 (2002). Medline doi:10.1101/gad.967302

29. A. M. Kringstein, F. M. Rossi, A. Hofmann, H. M. Blau, Graded transcriptional response to different concentrations of a single transactivator. *Proc. Natl. Acad. Sci. U.S.A.* **95**, 13670–13675 (1998). Medline doi:10.1073/pnas.95.23.13670

30. S. R. Biggar, G. R. Crabtree, Cell signaling can direct either binary or graded transcriptional responses. *EMBO J.* **20**, 3167–3176 (2001). Medline doi:10.1093/emboj/20.12.3167

31. J. Stewart-Ornstein, C. Nelson, J. DeRisi, J. S. Weissman, H. El-Samad, Msn2 coordinates a stoichiometric gene expression program. *Curr. Biol.* **23**, 2336–2345 (2013). Medline doi:10.1016/j.cub.2013.09.043

32. J. Song, A. Angel, M. Howard, C. Dean, Vernalization – a cold-induced epigenetic switch. *J. Cell Sci.* **125**, 3723–3731 (2012). Medline doi:10.1242/jcs.084764

33. M. Busslinger, A. Tarakhovsky, Epigenetic control of immunity. *Cold Spring Harb. Perspect. Biol.* **6**, a019307 (2014). Medline doi:10.1101/cshperspect.a019307

34. S. Tay, J. J. Hughey, T. K. Lee, T. Lipniacki, S. R. Quake, M. W. Covert, Single-cell NF-κB dynamics reveal digital activation and analogue information processing. *Nature* **466**, 267–271 (2010). Medline doi:10.1038/nature09145

35. N. Wakabayashi-Ito, S. Nagata, Characterization of the regulatory elements in the promoter of the human elongation factor-1α gene. *J. Biol. Chem.* **269**, 29831–29837 (1994). Medline

36. D. Sprinzak, A. Lakhanpal, L. Lebon, L. A. Santat, M. E. Fontes, G. A. Anderson, J. Garcia-Ojalvo, M. B. Elowitz, *Cis*-interactions between Notch and Delta generate mutually exclusive signalling states. *Nature* **465**, 86–90 (2010). Medline doi:10.1038/nature08959

37. W. Weber, C. Fux, M. Daoud-el Baba, B. Keller, C. C. Weber, B. P. Kramer, C. Heinzen, D. Aubel, J. E. Bailey, M. Fussenegger, Macrolide-based transgene control in mammalian cells and mice. *Nat. Biotechnol.* **20**, 901–907 (2002). Medline doi:10.1038/nbt731

38. N. Rosenfeld, J. W. Young, U. Alon, P. S. Swain, M. B. Elowitz, Gene regulation at the single-cell level. *Science* **307**, 1962–1965 (2005). Medline doi:10.1126/science.1106914

39. T. Li, J. F. Hu, X. Qiu, J. Ling, H. Chen, S. Wang, A. Hou, T. H. Vu, A. R. Hoffman, CTCF regulates allelic expression of *Igf2* by orchestrating a promoter-polycomb repressive complex 2 intrachromosomal loop. *Mol. Cell. Biol.* **28**, 6473–6482 (2008). Medline doi:10.1128/MCB.00204-08

40. I. B. Dodd, M. A. Micheelsen, K. Sneppen, G. Thon, Theoretical analysis of epigenetic cell memory by nucleosome modification. *Cell* **129**, 813–822 (2007). Medline doi:10.1016/j.cell.2007.02.053

41. A. Coulon, C. C. Chow, R. H. Singer, D. R. Larson, Eukaryotic transcriptional dynamics: From single molecules to cell populations. *Nat. Rev. Genet.* **14**, 572–584 (2013). Medline doi:10.1038/nrg3484

42. L. Cai, N. Friedman, X. S. Xie, Stochastic protein expression in individual cells at the single molecule level. *Nature* **440**, 358–362 (2006). Medline doi:10.1038/nature04599

43. W. J. Blake, M. KAErn, C. R. Cantor, J. J. Collins, Noise in eukaryotic gene expression. *Nature* **422**, 633–637 (2003). Medline doi:10.1038/nature01546

44. J. M. Raser, E. K. O'Shea, Noise in gene expression: Origins, consequences, and control. *Science* **309**, 2010–2013 (2005). Medline doi:10.1126/science.1105891

45. N. Friedman, L. Cai, X. S. Xie, Linking stochastic dynamics to population distribution: An analytical framework of gene expression. *Phys. Rev. Lett.* **97**, 168302 (2006). Medline doi:10.1103/PhysRevLett.97.168302

46. J. Boros, N. Arnoult, V. Stroobant, J.-F. Collet, A. Decottignies, Polycomb repressive complex 2 and H3K27me3 cooperate with H3K9 methylation to maintain heterochromatin protein 1α at chromatin. *Mol. Cell. Biol.* **34**, 3662–3674 (2014). Medline doi:10.1128/MCB.00205-14

47. D. Pasini, K. H. Hansen, J. Christensen, K. Agger, P. A. Cloos, K. Helin, Coordinated regulation of transcriptional repression by the RBP2 H3K4 demethylase and Polycomb-Repressive Complex 2. *Genes Dev.* **22**, 1345–1355 (2008). Medline doi:10.1101/gad.470008

48. D. Pasini, M. Malatesta, H. R. Jung, J. Walfridsson, A. Willer, L. Olsson, J. Skotte, A. Wutz, B. Porse, O. N. Jensen, K. Helin, Characterization of an antagonistic switch between histone H3 lysine 27 methylation and acetylation in the transcriptional regulation of Polycomb group target genes. *Nucleic Acids Res.* **38**, 4958–4969 (2010). Medline doi:10.1093/nar/gkq244

49. B. Jin, Y. Li, K. D. Robertson, DNA methylation: Superior or subordinate in the epigenetic hierarchy? *Genes Cancer* **2**, 607–617 (2011). Medline doi:10.1177/1947601910393957